Progress In Electromagnetics Research, Vol. 177, 75–84, 2023

Research on the Radiation Properties of Tapered Slot Magnetoelectric Antenna

Tianhao Han[1], Biao Dong[1], Yong Zhang[1], Yu Wang[1, 2], Zhongming Yan[1, 2], Hongcheng Zhou[1, 2, *], Jinhua Feng[1], and Yulong Liu[1]

Abstract—The advent of acoustically mediated magnetoelectric (ME) antennas offers a new idea for miniaturizing antennas. The ME antenna operates at mechanical resonant frequencies, so its dimension can be reduced by three orders of magnitude compared to an electric antenna counterpart. However, the poor directional radiation property of the reported magnetoelectric antennas, which is similar to an ideal magnetic dipole, limits the use of the ME antennas. In this paper, we propose a tapered slot magnetoelectric (TSME) antenna which is composited of PZT-5H and Metglas with dimensions of 50 mm × 30 mm × 0.596 mm and an operating frequency of around 30 kHz. Inspired by the structure of the slot-coupled antenna, the structure of the magnetostrictive layer of the ME antenna has been modified, and the front-back radiation difference in the near field has been improved by 7.9 dB compared to a normal ME antenna. The different operating principles between the TSME antenna and normal ME antennas have been analyzed and verified in the paper. In addition, we have successfully implemented amplitude modulation (AM) signals transmission using TSME antennas. This work provides new ideas for improving the radiation performance of ME antennas and lays the foundation for their practical application.

1. INTRODUCTION

"Bulk Acoustic Wave-Mediated Multiferroic Antennas" was first proposed by Yao et al. in 2015 [1]. The report demonstrated that piezoelectric-magnetostrictive composites film with the thicknesses of the order of 10^{-5} wavelength can achieve efficient radiation at GHz frequencies through theoretical derivation and simulation. This magnetoelectric (ME) antenna offers a completely new way to miniaturize antennas and has attracted widespread interest. In 2017, Nan et al. first reported magnetoelectric antennas operating at 60 MHz and 2.5 GHz, which demonstrated the feasibility of the technology [2]. Zaeimbashi et al.'s studies opened up the application of magnetoelectric antennas in the medical field, ultra-miniaturized ME antenna with a diameter of less than 200 µm, and ultra-compact dual-band smart NEMS ME antenna with a size of $250 \times 174\ \mu m^2$ which combine communication, electromagnetic energy harvesting, and static neuronal magnetic field detection capabilities [3, 4]. Yu et al. applied a ME antenna to a neurostimulation implants that can transmit over 1 mW of power wirelessly to a depth of 30 mm in the body [5]. Dong et al. reported a very-low-frequency (VLF) ME antenna operating at 23.95 kHz with a maximum communication distance of 120 m, which showed great promise for ME antenna applications in underground, underwater, and earth ionospheric waveguide communications [6]. Niu and Ren integrated a low-frequency (LF) ME antenna with a DC magnetic bias to achieve higher performance, which had an underwater communication range of 1.2 m and 17.96 times higher radiation efficiency than a spiral LF antenna [7, 8]. Apparently, ME antennas may also be used in portable

Received 8 March 2023, Accepted 30 May 2023, Scheduled 6 June 2023

* Corresponding author: Hongcheng Zhou (zhouhc@home.swjtu.edu.cn).

[1] School of Electrical Engineering, Southwest Jiaotong University, Chengdu 611756, China. [2] Key Laboratory of Magnetic Suspension Technology and Maglev Vehicle, Ministry of Education, Chengdu 611756, China.

communications and Internet of Things. However, simulation and experimental studies showed that the radiation patterns of the previously reported magnetoelectric antennas are similar to an ideal magnetic dipole [6, 9, 10]. As a result, ME antennas have almost no capability for directional radiation. Antennas with good directionality have several advantages including enhanced capacity of the network, longer range of transmission, better spatial reuse, and lower interference [11]. Electromagnetic radiation of antenna outside the target direction may cause electromagnetic compatibility problems and even damage the equipment. Because of these, improving directionality is an indispensable part of antenna design.

Vivaldi antenna is a widely used slot-coupled antenna, which has attracted the utmost attention from researchers owing to its high gain, wide bandwidth, and stable radiation properties [11–13]. Using the structure of Vivaldi antenna for reference, we design a tapered slot magnetoelectric (TSME) antenna by adding a tapered slot in the magnetostrictive layer of a ME antenna for the first time. The TSME antenna operates at a mechanical resonance of 29.8 kHz. The directionality of the TSME antenna is enhanced significantly compared with prior researches on ME antenna. This work verifies the feasibility of applying the traditional antenna design method to the ME antenna design. Furthermore, we investigate the amplitude modulated (AM) signal transmission capability of the TSME antenna.

2. DEVICE DESIGN AND SIMULATION ANALYSIS

2.1. Antenna Structure Design and Operation Principle

In this paper, we design a tapered slot magnetoelectric (TSME) antenna as shown in Figure 1. The cyan part is piezoelectric material PZT-5H, which has dimensions of $L_e = 50\,\text{mm}$, $W_e = 30\,\text{mm}$, and $T_e = 0.46\,\text{mm}$, and is polarized along the thickness direction. The red part shown in Figure 1 is magnetostrictive material FeBSiC (Metglas) with dimensions of $L_m = 47\,\text{mm}$, $W_m = 30\,\text{mm}$, and $T_m = 0.136\,\text{mm}$. There is a tapered slot designed on the layer of Metglas, and the edges of the tapered slot are defined by an exponential function. The width W_1 of the narrowest part of the slots is 0.2 mm, and the width W_2 of the widest part is 24 mm. The Metglas layer is divided into two parts by the slot. The easy axes of magnetization of the two parts parallel to x-axis and magnetization directions are antiparallel. In addition, the part of PZT-5H not covered with Metglas is used for connecting the feeder.

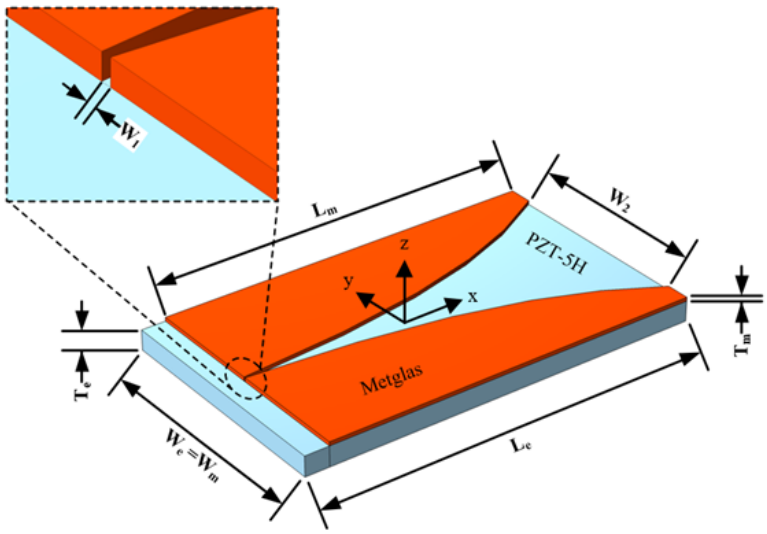

Figure 1. The structure diagram of TSME antenna.

Though the design of TSME antenna learns from Vivaldi antenna, their operation principles are different. TSME antennas radiate through the piezoelectric and magnetostrictive effects, and (1) and (2) are the piezoelectric constitutive equations and the piezomagnetic constitutive equations,

respectively, [14–17],

$$\begin{cases} T = c_E S - e_E^T E \\ D = e_E S + \varepsilon_S E \end{cases} \tag{1}$$

$$\begin{cases} T = c_H S - e_H^T H \\ B = e_H S + \mu_S H \end{cases} \tag{2}$$

where T and S symbolize the stress and strain tensors; E and D symbolize the electric field intensity and electric displacement vectors; c_E is the stiffness tensor of the piezoelectric material; e_E is the piezoelectric stress constant tensor; ε_S is the dielectric constant tensor; H and B symbolize the magnetic field intensity and magnetic flux density vectors; c_H is the stiffness tensor of the piezomagnetic material; e_H is the piezomagnetic stress constant tensor; and μ_S is the permeability tensor. When transmitting signals, the antenna mainly utilizes converse piezoelectric effect and converse magnetostrictive effect, and the vibration mode is length expansion vibration. For the convenience of analysis, the equations can be simplified as (3) and (4).

$$\begin{cases} T_{xx} = -e_{Exz}^T E_z \\ D_z = \varepsilon_{Szz} E_z \end{cases} \tag{3}$$

$$\begin{cases} T_{xx} = c_{Hxx} S_{xx} \\ B_x = e_{Hxx} S_{xx} \end{cases} \tag{4}$$

The alternating voltage applied to the upper and lower surfaces of the piezoelectric layer creates a z-directional electric field E_z inside the piezoelectric layer and causes length expansion vibration through the converse piezoelectric effect. The vibration stress T_{xx} and strain S_{xx} in magnetostrictive layer generate the alternating magnetic field B_x through the converse magnetostrictive effect. Due to the antiparallel magnetization directions, the piezomagnetic stress constants e_{Hxx} of the two parts of the magnetostrictive layer are opposite. As a result, it can be inferred from (4) that the directions of the magnetic flux density B_x generated by the two parts are opposite. The tapered slot plays a role in adjusting the magnetic circuit and guiding magnetic field radiation. Next, we analyze the radiation properties of TSME antenna through simulations.

2.2. Simulations of TSME Antennas and Normal ME Antenna

In order to study the radiation properties of the TSME antenna and the influence of the tapered slot area on the radiation, we design four TSME antennas with different slot dimensions for simulation analysis, and the software used for the simulations is COMSOL. The slot lines of the TSME antennas are defined by the exponential functions in Table 1. The slot area increases gradually from ANT1 to ANT4, and the magnetization directions of the two parts of Metglas are antiparallel. Additionally, a normal ME antenna ANT0 with no tapered slot is designed for the comparison with the TSME antennas. The resonant frequencies of extension vibration along length can be estimated by (5), where L is the length of the antennas, ρ the effective mass density, s_{xx} the effective compliance constant. ρ and s_{xx} are the averages of the parameters of PZT-5H and Metglas weighted by volume ratio r_e and r_m, as shown in (6)

Table 1. Functions of tapered slot edge curves.

Antenna	Function	Area of slot
ANT1	$y = 0.001 \cdot e^{(0.2 \cdot x)} + 0.099$	$130.18\,\text{mm}^2$
ANT2	$y = 0.043 \cdot e^{(0.12 \cdot x)} + 0.057$	$206.36\,\text{mm}^2$
ANT3	$y = 0.11 \cdot e^{(0.1 \cdot x)} - 0.01$	$238.74\,\text{mm}^2$
ANT4	$y = 1.26 \cdot e^{(0.05 \cdot x)} - 1.16$	$369.03\,\text{mm}^2$

The value range of x in curve functions is 0–47 mm.

and (7).

$$f_r = \frac{1}{2L}\sqrt{\frac{1}{\rho s_{xx}}} \tag{5}$$

$$\rho = \rho_e \cdot r_e + \rho_m \cdot r_m \tag{6}$$

$$s_{xx} = \frac{s_{Exx} \cdot s_{Hxx}}{s_{Hxx} \cdot r_e + s_{Exx} \cdot r_m} \tag{7}$$

The parameters of the PZT-5H are $\rho_e = 7600\,\mathrm{kg/m^3}$ and $s_{Exx} = 17 \times 10^{-12}\,\mathrm{m^2/N}$, and those of Metglas are $\rho_m = 7180\,\mathrm{kg/m^3}$ and $s_{Hxx} = 10.95 \times 10^{-12}\,\mathrm{m^2/N}$. According to (5)–(7), the estimated resonant frequencies of ANT0–ANT4 are 29.71 kHz, 29.58 kHz, 29.51 kHz, 29.47 kHz, and 29.34 kHz, respectively, while the simulated results are 29.89 kHz, 30.28 kHz, 30.22 kHz, 30.14 kHz, and 29.70 kHz, respectively. The difference in resonant frequencies is due to the inhomogeneous distribution of the Metglas.

It can be seen from Figure 2(a) that the vibration of ANT1 is mainly longitudinal length extension vibration, and it is mirror-symmetrical along the straight-line $y = 0$. In Figure 2(b), the magnetic flux density directions of the two parts of the magnetostrictive layer are opposite. The symmetry of stress and the antisymmetry of magnetic flux density can be seen intuitively in Figure 2(c). The simulated results of the other TSME antennas are similar to ANT1. The vibration and magnetic flux density of the TSME antenna in the simulations demonstrate that its mode of operation conforms to design expectations.

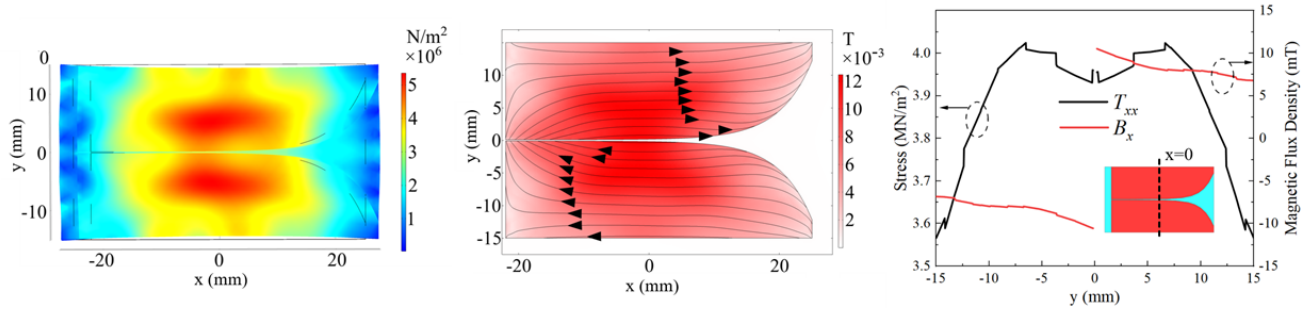

Figure 2. Vibration stress and magnetic flux density of ANT1 at resonant frequency. (a) Stress diagram of ANT1; (b) Magnetic flux density of magnetostrictive layer; (c) The stress and magnetic flux density of the magnetostrictive layer on the straight-line $x = 0$.

Figure 3 indicates the simulated near-field magnetic field patterns of the five antennas. ANT0 has almost the same radiation properties in near-field on xOy and xOz planes which are very similar to an ideal magnetic dipole. The maximum radiation direction of ANT0 is 0° on both planes, and the radiation at 0° is 0.24 dB larger than 180° which means that its directionality is weak. The simulated near-field magnetic field patterns of the four TSME antennas are similar. On the xOy plane, the maximum radiation directions of ANT1–ANT4 are 52.5° and 307.5°. At 0°, the radiation of the TSME antennas is about 4.8 dB less than that at 52.5° or 307.5°, and the minimum radiation direction is 180°. On the xOz plane, the maximum radiation of the four TSME antennas is in the direction of 0°. However, ANT1 has a sub-maximum radiation at 180°, which is significantly different from the other three antennas. The radiation difference of ANT1 between 0° and 180° is 22 dB, while ANT2–ANT4 is around 26–27 dB. The front-back differences of the TSME antennas increase with the increase of the slot area. When the slot area exceeds 200 $\mathrm{mm^2}$, the front-back difference of TSME antenna no longer changes drastically. The slot area of ANT1 that is too small causes a greater amount of backward radiation, which weakens the directionality. ANT4 has the best directionality, whose front-back radiation difference is 27 dB. It can be seen that the TSME antennas have significant better directionality than ANT0 in the near field and are different from the ideal magnetic dipole.

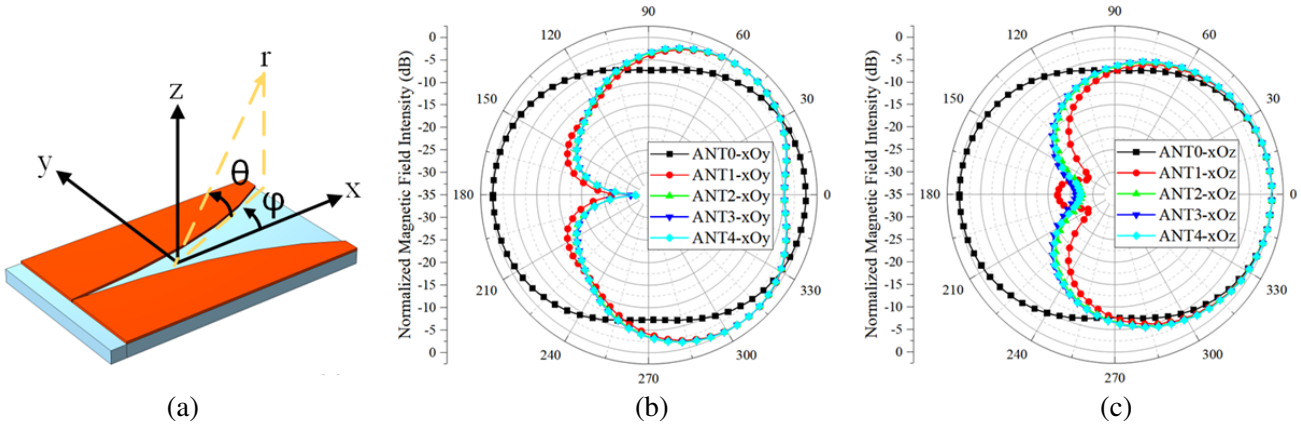

Figure 3. (a) The near-field normalized magnetic field patterns (15 cm from the antenna center) of the TSME antennas obtained by simulations. (b) Magnetic field patterns of xOy plane. (c) Magnetic field patterns of xOz plane. 0° is the direction of the positive axis x.

3. DEVICE FABRICATION AND TESTS

3.1. Fabrication of TSME Antenna and Normal ME Antenna

According to the simulated results shown in Figure 3, ANT4 has the best directionality, so it is fabricated for experimental verification, and ANT0 is fabricated for comparison. The prototypes of ANT0 and ANT4 are shown in Figures 4(a)–(b), respectively. PZT-5H and Metglas are bonded with epoxy, and the top and bottom surfaces of PZT-5H are connected with the inner conductor and outer conductor of the coaxial line, respectively. Due to the nonlinear relationship between the magnetostriction of Metglas and the external magnetic field [18–20], there should be a bias magnetic field to maximize the piezomagnetic coefficient e_{Hxx} of it. We use two magnets to provide a bias magnetic field for the antennas. As shown in Figure 4(c), an antenna fixator is used to fix the antennas and magnets, which includes three parts: top cap, support, and base, and a magnet slot is designed in the support part to fix the magnets.

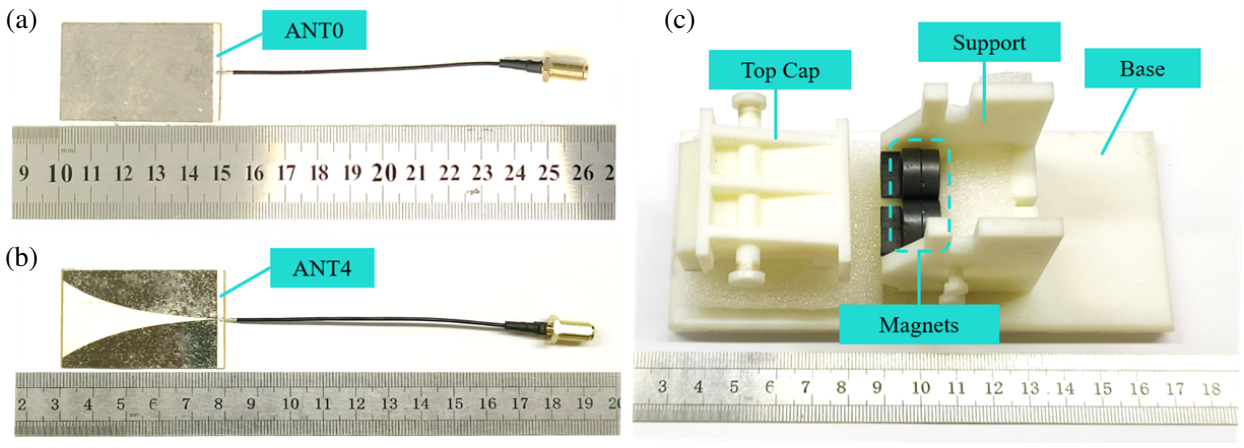

Figure 4. Prototypes of antennas and antenna fixator. (a) Normal ME antenna (ANT0); (b) TSME antenna (ANT4); (c) Antenna fixator.

3.2. TSME Antenna and Normal ME Antenna Properties Tests

The normalized output voltage of the coil shown in Figure 5(a) is obtained by transmitting sinusoidal signals with ANT0 and ANT4 and receiving signals with a 100-turn coil that is 15 cm away from the antenna. The actual resonant frequencies of the two antennas can be obtained by Figure 5(a), which are 30.4 kHz and 29.8 kHz. The differences between experimental and simulated results are caused by manufacturing error. The voltage reflection coefficients of ANT0 and ANT4 are tested by an network analyzer (SP809B, Prosund Electronic Technology Inc.), as shown in Figure 5(b). The minimum values of the voltage reflection coefficients of the two antennas are −13 dB and −12.8 dB, and the minimum value is not at the resonance frequency, which means that the impedance matching between the antenna and the excitation source at the resonance frequency has not reached the best.

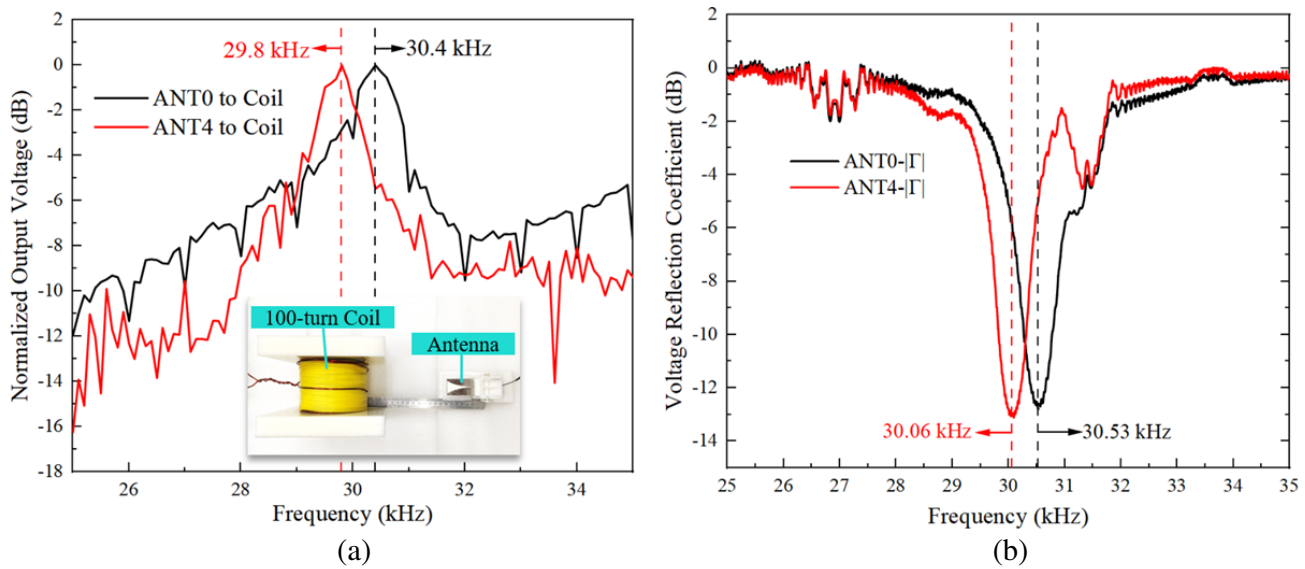

Figure 5. (a) Normalized output voltage of coil with ANT0 and ANT4 as transmitters, and the inset is the experimental photograph; (b) Voltage reflection coefficient of ANT0 and ANT4.

Figure 6(a) is the near-field magnetic field measurement system of ME antenna, including a function generator (DG1022U, Rigol Technology Inc.), a 60-turn coil, two voltage amplifiers, two filters, and an oscilloscope (MSOX3024T, Keysight Technology Inc.). The function generator applies alternating voltage to the antenna. The coil is placed on a circle with a radius of 15 cm, and the antenna is placed at the center of the circle. The voltage amplifiers can amplify the voltage signal induced by the coil by 80 dB, and the filters can filter high-frequency noise above 1 MHz, and the received signal is captured by the oscilloscope.

The experimental results in Figures 6(b)–(c) show that the front-back radiation differences of ANT0 on the xOy and xOz planes are only 3.2 dB and 3.9 dB, respectively, and ANT4 are 11.09 dB and 9.25 dB, respectively. ANT4 exhibits a stronger directionality. The actual front-back radiation difference of ANT4 is smaller than the simulation results, which may be due to the inhomogeneous magnetization of Metglas under the bias magnetic field. Figure 6(h) shows the magnetization of the Metglas under the bias magnetic field in the static magnetic field simulation, and the magnetization on its right side is significantly smaller than that on the left side, which leads to the fact that the piezomagnetic coefficient of the Metglas in the right region does not reach the maximum, thus leading to the reduction of the forward radiation of the antenna.

The magnetic field components of ANT0 on xOy plane are mainly φ-directional and r-directional components, and on xOz plane are mainly θ-directional and r-directional components, as shown in Figures 6(d)–(e). Also, the experimental and simulated results of ANT0 are in good agreement. The magnetic field components of ANT4 on xOy plane are mainly φ-directional and r-directional

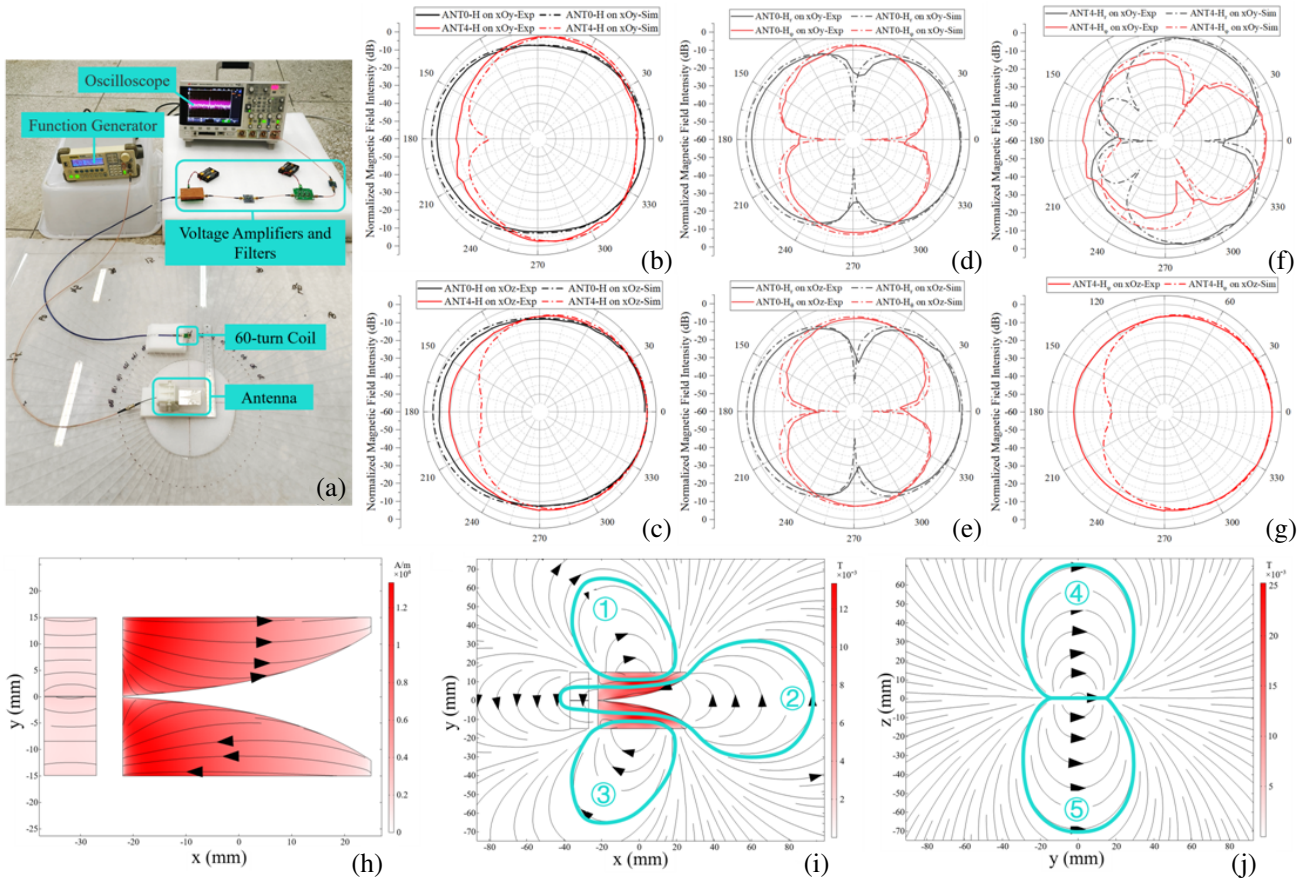

Figure 6. (a) Near-field magnetic field testing system; (b) Normalized H of ANT0 and ANT4 on xOy plane; (c) Normalized H of ANT0 and ANT4 on xOz plane; (d) Normalized H_φ and H_r of ANT0 on xOy plane; (e) Normalized H_θ and H_r of ANT0 on xOz plane; (f) Normalized H_φ and H_r of ANT4 on xOy plane; (g) Normalized H_φ of ANT4 on xOz plane; (h) Magnetization of Metglas under bias magnetic field in simulation; (i) Magnetic field of ANT4 on xOy plane; (j) Magnetic field of ANT4 on yOz plane.

components, and on xOz plane are almost exclusively φ-directional component, as shown in Figures 6(f)–(g). In Figure 6(f), H_r and H_φ in experiment are missing 1 and 2 minima respectively compared to the simulation results. A similar situation occurs with H_φ in Figure 6(g). The bias magnetic field causes a large y-directional component of the magnetization to the left of Metglas as shown in Figure 6(h), which increases its backward H_φ and H_r in the 131.8° and 228.2° directions. The magnetic field components not shown in Figures 6(d)–(g) are much smaller than the others. It is clear that the radiation pattern of ANT0 is similar to that of an ideal magnetic dipole, while the radiation pattern of ANT4 is significantly different from that of ANT0.

It can be seen from the experimental results, the unique structure of the TSME antenna is inspired by slot-coupled antenna, which makes its radiation pattern different from that of the reported magnetoelectric antennas, and its near field exhibits a better directionality than the normal ME antenna. What cannot be ignored is that the directionality of the TSME antenna has the potential to be improved by optimizing the bias field and structure.

The magnetic field generated by ANT4 forms five main magnetic loops as shown in Figures 6(i)–(j). In an ideal situation, only magnetic loop 2 should exist in ANT4, with the other magnetic loops being constrained in the Metglas and the magnetic field being guided forward by the tapered slot. In practical tests, magnetic loops 1 and 3 produce side radiation on xOy plane, and magnetic loops 4 and 5 produce side radiation on xOz plane. Therefore, reducing the magnetic field in the loops other than magnetic

loop 2 and concentrating the magnetic field in magnetic loop 2 is the key to improving the directionality of the TSME antenna.

Furthermore, since modulated signals are often required in information transmission, the feasibility of AM signal transmission with the TSME antenna has been experimentally analyzed. In the experiments, ANT4 is used to transmit signals, and a coil is used to receive them, as shown in the inset of Figure 5(a). The received signals are demodulated using non-coherent demodulation. The carrier frequency of the original AM signal in the experiment is 29.8 kHz; the modulation depth is 100%; and the modulation frequencies are 100 Hz, 500 Hz, and 1 kHz. Figure 7 shows the received signals waveform and demodulated signals waveform of the coil. The coil successfully received the three modulated signals from ANT4 and demodulated the corresponding sinusoidal waveforms. It can be seen from Table 2 that as the modulation frequency increases, the modulation depth of the received signal gradually decreases, which leads to a decrease in the amplitude of the demodulated signal. The AM signal contains three frequency components: the carrier frequency ω_c, the difference between the carrier frequency and the modulating frequency ω_d, and the sum of the carrier frequency and the modulating frequency ω_s. As the modulation frequency increases, ω_d and ω_s gradually move away from the carrier frequency, and it can be seen from Figure 5(a) that the radiation performance of the TSME antenna at these two frequencies decreases, which results in the reduction in modulation depth.

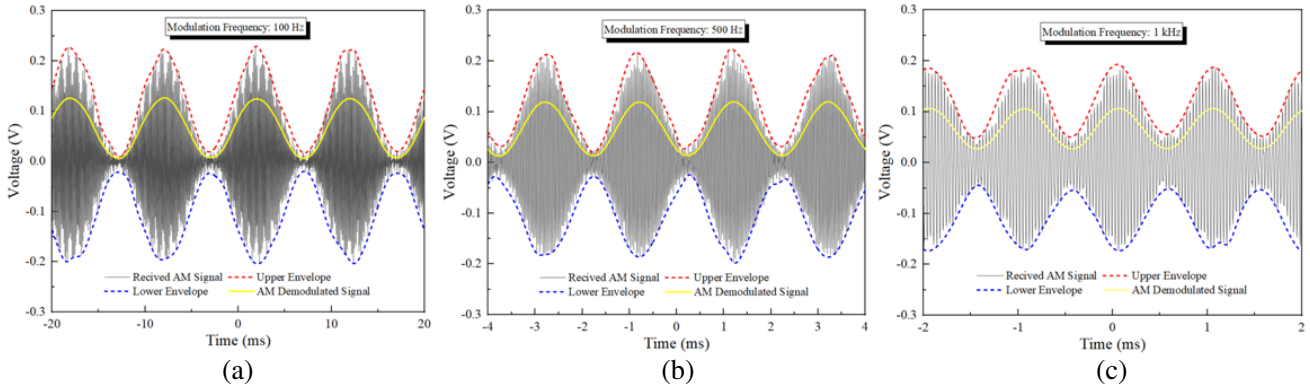

Figure 7. AM signals received by coil and their envelopes and demodulation signals. (a) Signals with modulation frequency of 100 Hz; (b) Signals with modulation frequency of 500 Hz; (c) Signals with modulation frequency of 1 kHz.

Table 2. Properties of AM signals received by coil.

Modulation Frequency	Modulation Depth	Amplitude of Demodulated Signal
100 Hz	84.4%	0.0591 V
500 Hz	61.5%	0.0528 V
1 kHz	55.6%	0.0396 V

The TSME antenna demonstrates that it is feasible to improve the performance of magnetoelectric antennas by introducing conventional antenna structures. The dimensions of the TSME antenna are six orders of magnitude less than the wavelength of electromagnetic wave at its operating frequency which is much smaller than the conventional antennas. Due to the good directionality of TSME antenna, it can be used in the communication system of bio-implantable devices to reduce the damage to surrounding biological tissue caused by electromagnetic radiation. In addition, the arraying of TSME antennas holds the promise of high-power directional transmission and applications for long-range, underwater, underground communications and detection.

4. CONCLUSION

A novel structure of the magnetoelectrical antenna is designed in this paper. The magnetostrictive layer of the TSME antenna is divided into two parts by the tapered slot, and the magnetization axes are antiparallel. The tapered slot guides the magnetic field to radiate towards its opening direction, so that the TSME antenna can realize directional radiation in near-field. And its operating principle is verified by finite element simulations. The radiation mode of TSME antenna is different from that of normal ME antenna. TSME antenna has better radiation directivity than the normal ME antenna, and its dimension is three orders smaller than that of the conventional antenna, which means that TSME antenna has the hope of becoming a revolutionary device to replace the traditional long-wave antenna.

REFERENCES

1. Yao, Z., Y. E. Wang, S. Keller, et al., "Bulk acoustic wave-mediated multiferroic antennas: Architecture and performance bound," *IEEE Transactions on Antennas and Propagation*, Vol. 63, No. 8, 3335–3344, Aug. 2015.
2. Nan, T. X., H. Lin, Y. Gao, et al., "Acoustically actuated ultra-compact NEMS magnetoelectric antennas," *Nature Communications*, Vol. 8, 296, Aug. 22, 2017.
3. Zaeimbashi, M., H. Lin, C. Dong, et al., "NanoNeuroRFID: A wireless implantable device based on magnetoelectric antennas," *IEEE Journal of Electromagnetics, RF, and Microwaves in Medicine and Biology*, Vol. 3, No. 3, 206–215, Sept. 2019.
4. Zaeimbashi, M., M. Nasrollahpour, A. Khalifa, et al., "Ultra-compact dual-band smart NEMS magnetoelectric antennas for simultaneous wireless energy harvesting and magnetic field sensing," *Nature Communications*, Vol. 12, No. 1, Article number: 3141, May 25, 2021.
5. Yu, Z. H., J. C. Chen, F. T. Alrashdan, et al., "MagNI: A magnetoelectrically powered and controlled wireless neurostimulating implant," *IEEE Transactions on Biomedical Circuits and Systems*, Vol. 14, No. 6, 1241–1252, Dec. 2020.
6. Dong, C. Z., Y. F. He, M. H. Li, et al., "A portable very low frequency (VLF) communication system based on acoustically actuated magnetoelectric antennas," *IEEE Antennas and Wireless Propagation Letters*, Vol. 19, No. 3, 398–402, Mar. 2020.
7. Niu, Y. P. and H. Ren, "A miniaturized low frequency (LF) magnetoelectric receiving antenna with an integrated DC magnetic bias," *Applied Physics Letters*, Vol. 118, No. 26, Jun. 28, 2021.
8. Niu, Y. P. and H. Ren, "Transceiving signals by mechanical resonance: A miniaturized standalone low frequency (LF) magnetoelectric mechanical antenna pair with integrated DC magnetic bias," *IEEE Sensors Journal*, Vol. 22, No. 14, 14008–14017, Jul. 15, 2022.
9. Xu, J. R., C. M. Leung, X. Zhuang, et al., "A low frequency mechanical transmitter based on magnetoelectric heterostructures operated at their resonance frequency," *Sensors*, Vol. 19, No. 4, 853, Feb. 2, 2019.
10. Xu, G. K., S. Q. Xiao, Y. Li, et al., "Modeling of electromagnetic radiation-induced from a magnetostrictive/piezoelectric laminated composite," *Physics Letters A*, Vol. 385, 126959, Jan. 7, 2021.
11. George, R. and T. A. J. Mary, "Review on directional antenna for wireless sensor network applications," *IET Communications*, Vol. 14, No. 5, 715–722, Mar. 17, 2020.
12. Bhattacharjee, A., A. Bhawal, A. Karmakar, et al., "Vivaldi antennas: A historical review and current state of art," *International Journal of Microwave and Wireless Technologies*, Vol. 13, No. 8, 833–850, Oct. 2021.
13. Mehdipour, A., K. Mohammadpour-Aghdam, and R. Faraji-Dana, "Complete dispersion analysis of Vivaldi antenna for ultra wideband applications," *Progress In Electromagnetics Research*, Vol. 77, 85–96, 2007.
14. Will-Cole, A. R., A. E. Hassanien, S. D. Calisgan, et al., "Tutorial: Piezoelectric and magnetoelectric N/MEMS-materials, devices, and applications," *Journal of Applied Physics*, Vol. 131, No. 24, 241101-1–32, Jun. 28, 2022.

15. Tichý, J., J. Erhart, E. Kittinger, and J. Přívratská, "Piezoelectric properties," *Fundamentals of Piezoelectric Sensorics*, 69–100, Springer, 2010.
16. Berlincourt, D. A., "Piezoelectric and piezomagnetic materials and their function in transducers," *Physical Acoustics*, Vol. 1, 169–270, 1964.
17. Li, N., X. Y. Li, B. N. Xu, et al., "Design and optimization of a micron-scale magnetoelectric antenna based on acoustic excitation," *Micromachines*, Vol. 13, No. 10, Oct. 2022.
18. Lou, J., R. E. Insignares, Z. Cai, et al., "Soft magnetism, magnetostriction, and microwave properties of FeGaB thin films," *Applied Physics Letters*, Vol. 91, 182504-1–3, Oct. 29, 2007.
19. Zhai, J., Z. Xing, S. Dong, et al., "Magnetoelectric laminate composites: An overview," *Journal of the American Ceramic Society*, Vol. 91, No. 2, 351–358, Feb. 2008.
20. Zhai, J. Y., S. X. Dong, Z. P. Xing, et al., "Giant magnetoelectric effect in Metglas/polyvinylidene-fluoride laminates," *Applied Physics Letters*, Vol. 89, No. 8, Aug. 21, 2006.